Available online at www.sciencedirect.com

ScienceDirect

Proceedings of the Combustion Institute 37 (2019) 5129–5136

Proceedings of the Combustion Institute

www.elsevier.com/locate/proci

Characteristics of self-excited spinning azimuthal modes in an annular combustor with turbulent premixed bluff-body flames

Marek Mazur*, Håkon T. Nygård, James R. Dawson, Nicholas A. Worth

Department of Energy and Process Engineering, Norwegian University of Science and Technology, N-7491 Trondheim, Norway, Kolbjørn Hejes v 1B, Trondheim 7491, Norway

Received 30 November 2017; accepted 16 July 2018
Available online 23 August 2018

Abstract

In this paper we investigate self-excited azimuthal modes in an annular combustor with turbulent premixed bluff-body stabilised flames. Previous studies have shown that both swirl and equivalence ratio influence modal dynamics, i.e. the time-varying nature of the modes. However, self-excited azimuthal modes have not yet been investigated in turbulent flames without bulk swirl, which do not generate any preferential flow in either azimuthal direction, and may therefore lead to different behaviour. Joint probability density functions of the instability amplitudes at various flowrates and equivalence ratios showed a strong bi-modal response favouring both ACW and CW spinning states not previously observed. Operating conditions leading to a bi-modal response provide a unique opportunity to investigate whether the structure of the global fluctuating heat release rate of self-excited spinning modes in both directions exhibit similar dynamics and structure. This was investigated using high-speed OH* chemiluminescence images of the annular combustor and a new rotational averaging method was applied which decomposes the spinning components of the global fluctuating heat release rate. The new rotational averaging, which differs from standard phase-averaging, produces spatial averages in a frame of reference moving with the spinning wave. The results show that the structure of the fluctuating heat release rate for spinning modes is highly asymmetric as characterised by large, crescent shaped regions of high OH* intensity, located on the far side of each flame, relative to the direction of the azimuthally propagating pressure wave. In comparison with interacting swirling flames, these results indicate that the previously observed radial asymmetry of OH* fluctuations may be introduced through advection by local swirl.

Keywords: Flame dynamics; Combustion instability; Annular combustor; Azimuthal modes; Modal dynamics

* Corresponding author.
E-mail address: marek.mazur@ntnu.no (M. Mazur).

https://doi.org/10.1016/j.proci.2018.07.080

1. Introduction

Thermoacoustic instabilities remain a crucial impediment in the design and operation of low emission combustors in aeroengines and gas turbines for power generation. Many gas turbines use annular combustor geometries which give rise to self-excited azimuthal modes [6].

Recent studies have provided new insight into azimuthal modes and have shown that due to azimuthal symmetry, self-excited instabilities in these systems give rise to more complex behaviour [1,2,4,7–10] compared with longitudinal modes in isolated single flame systems. Depending on the burner geometry, equivalence ratio and bulk velocity, the system can excite specific azimuthal modes or exhibit modal dynamics. Other investigations in annular combustors with turbulent swirling flames give rise to modal dynamics where, at a given operating point, the excited mode exhibits time-varying phase and amplitude, switching back and forth between spinning, standing and mixed modes [1–4,8,10]. In theoretical studies it was suggested, that this mode switching is related to the asymmetries in the heat release rate or flow [11–13].

So far, the occurrence of modal dynamics has only been observed in annular combustors equipped with turbulent swirling flames. Identical swirling injectors imparts mean azimuthal flow patterns which has an influence on the modal dynamics [3]. Bauerheim et al. [18] developed an analytical model demonstrating that changing the burner geometry breaks the azimuthal symmetry and promotes standing waves but the addition of even a small level bulk swirl promotes spinning modes. Bourgouin et al. [14] modified the annular combustor presented in Bourgouin et al. [2] by replacing swirling injectors with laminar matrix burners thereby removing any mean azimuthal flow components but demonstrated that spinning modes could be excited. Using the same configuration, Prieur et al. [17] showed that spinning, standing or slanted azimuthal modes were self-excited depending on the operating point but at certain conditions mode selection was very sensitive as hysteresis effects were observed. To date, the effect of turbulent premixed flames without swirl on the modal dynamics of self-excited azimuthal modes have yet to be investigated. Based on the limited information available, we are interested in knowing whether the absence of swirl and bulk azimuthal flow will result in a suppression of modal dynamics or, if modal dynamics occur, will they exhibit any statistical modal preference.

The aim of the present investigation is twofold: (i) to demonstrate the occurrence of self-excited azimuthal modes in an annular combustor equipped with bluff-body stabilised turbulent premixed flames without swirl and characterise their modal response for a range of operating conditions and, (ii) take advantage of the absence of swirl to better understand the fundamental response of the global fluctuating heat release rate in terms of its structure and dynamics when undergoing self-excited spinning modes. Insight into the modal response of turbulent premixed flames without swirl and associated structure dynamics of the heat release rate are required to gain a more complete understanding of combustion instabilities in annular combustors.

2. Experimental methods

2.1. Annular combustor

The experiments were carried out in an atmospheric annular combustor developed previously [3–5]. Figure 1 shows a 3D model of the annular combustor. It consists of a plenum, which is fed by premixed ethylene-air mixtures, and contains a grid and a honeycomb for flow conditioning and a hemispherical body in the upper part of the plenum is used to divide the flow. The reactants are fed into the combustor through 12 injector tubes of diameter = 18.5 mm, fitted with a flush-mounted bluff body with a blockage ratio of 50%. A top view of the 12 bluff bodies is shown to the right of Fig. 1. The annular combustion chamber has an inner wall of diameter $D_i = 127$ mm and outer wall diameter $D_o = 212$ mm. The length of the inner and outer walls, $L_i = 130$ mm and $L_o = 300$ mm respectively, are mismatched to obtain self-excited instabilities as reported in [2–4]. Stability maps were obtained by varying the bulk exit velocity U_b, (calculated at the dump plane from the volumetric flow rate), in 0.6 m/s steps between $U_b = 17.7 - 21.1$ m/s. The equivalence ratio, ϕ, was varied in steps of 0.05 between $\phi = 0.7 - 1.0$. The power therefore varied between $82 - 194$ kW.

2.2. Experimental measurements

Pressure and OH* chemiluminescence measurements were obtained simultaneously. Dynamic pressures were measured by pairs of pressure sensors located upstream of the combustion chamber as shown in Fig. 1 at circumferential positions *p1, p2* and *p3*. The Kulite pressure sensors, model XCS-093s with a measurement sensitivity of 4.2857×10^{-3} mV/Pa, were connected to Fylde FE-579-TA bridge amplifiers and measurements were recorded with a sampling frequency of 51.2 kHz for a duration of 10 s, giving a frequency resolution of 0.1 Hz. Each measurement was repeated a total of 4 times across a range of inlet velocities, and for $U_b = 19.9$ m/s case, each measurement was repeated 40 times in order to report statistically resolved distributions of the modal preference. Between measurements the rig was reignited to ensure independence, removing the possibility of hysteresis. A wall mounted thermocouple ensured that

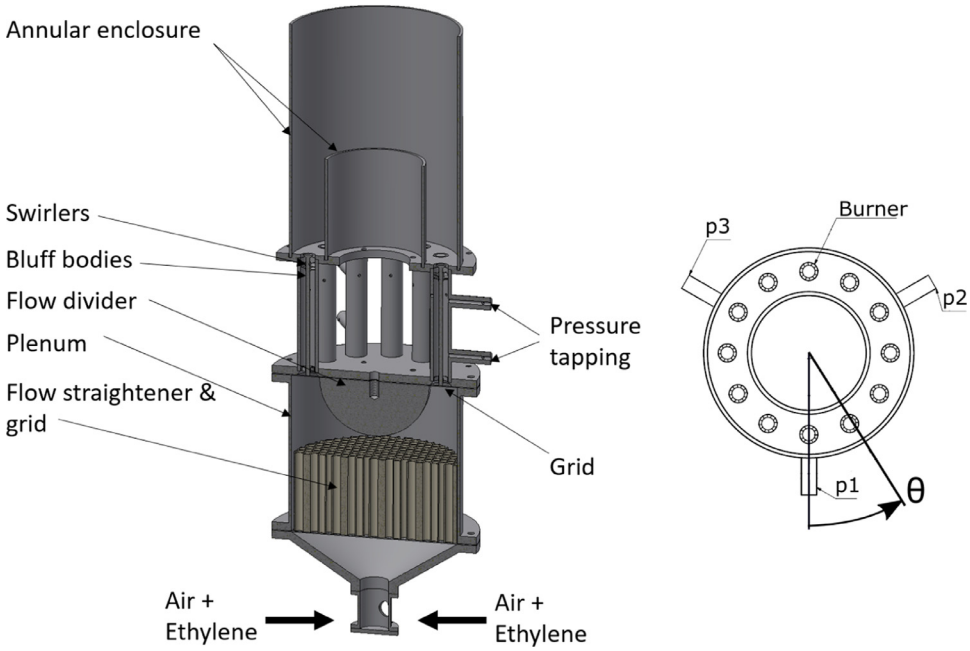

Fig. 1. Left: 3D model of the annular combustor with labels describing the main geometrical features. Right: Top view of the annular combustor showing the burner spacing and circumferential locations of the pressure measurements.

the combustor temperature was in the same range during each measurement. It should be noted that the JPDF distributions show little change varying the number of independent samples between 4 and 40, and can therefore be considered resolved for the current combustor setup.

To measure the structure of the fluctuating heat release rate around the annulus, high speed OH* chemiluminescence images were obtained from above using an air cooled mirror (As shown in [3]). A Phantom V2012 camera equipped with a LaVision IRO unit and a UV filter (model: D20-VG0035942) with a center wavelength of 310 nm and a full width at half maximum of 10 nm was used. A total of 120,000 images (full camera memory) was acquired at a sampling frequency of 10 kHz and using an array of 768 × 768 pixels, giving a spatial resolution of 0.31 mm/pixel. Triggering and measurements were recorded using a 24 bit NI Compact DAQ system, model 9174.

2.3. Analysis of the pressure data

To evaluate the self-excited modes the procedure described in previous papers was used [3,5,8,10]. Measurement positions of the pressure sensors, *p1, p2* and *p3*, were separated by $\theta = 120^\circ$ as shown in Fig. 1. We assume the modes correspond to a superposition of one-dimensional plane waves according to: $p(\theta_k, t) = [A_+ e^{i(\theta_k - \nu t/R)} + A_- e^{i(-\theta_k + \nu t/R)}]e^{i\omega_0 t}$ where A_+ and A_- are the amplitudes of anticlockwise (ACW) and clockwise (CW) waves respectively, ω is the angular frequency, and $v_\theta t/R$ is a lumped parameter that defines the angular velocity of the nodal line when both A_+ and $A_- > 0$.

The measured pressure is the real part of the complex pressure, $p_{\text{meas}} = Re(p)$. A least-squares fit over 6 cycles is used to evaluate the amplitudes A_+ and A_-, as well as the lumped parameter $\theta_P = v_\theta t/R$. The amplitude of the pressure fluctuations of any given mode is given by $[A_+^2 + A_-^2]^{1/2}$. A_+ and A_- are also used to calculate the spin ratio (SR) defined by Bourgouin et al. [2]: $SR = (|A_+| - |A_-|)/(|A_+| + |A_-|)$, where a $SR = \pm 1$ correspond to perfect spinning modes in the ACW and CW directions respectively, a $SR = 0$ corresponds to a standing wave and intermediate values are mixed modes.

2.4. Rotational averaging method for OH*

Due to the time-varying nature of the modes, conditional averaging is required for investigating the structure of the OH* fluctuations for different modes. OH* images are conditioned on the SR evaluated from the pressure time-series data. Since the SR varies in time, we must resort to choosing suitable thresholds of the SR to classify the modes into spinning and standing. In the present work OH* images are conditioned using the following thresholds and then phase-averaged [3,5,8]: $SR > 1/3$ are classified as ACW spinning modes, $SR < -1/3$ are classified as CW spinning modes, intermediate values are classed as standing modes $-1/3 < SR <$

1/3. The large imaging data set allowed a minimum of 500 images to be used at each phase angle even after conditional averaging to ensure convergence. In this paper we focus on spinning modes and are particularly interested in determining whether the structure of the OH* fluctuations is affected by the spin direction as found in swirling flames [3]. It is reasonable to expect that in the absence of swirl and bulk azimuthal flow the structure of the OH* fluctuations should be similar for modes spinning in either direction.

Since perfect spinning modes rarely occur and due to the presence of mode switching (described in 3.4), conditionally averaged spinning modes are more accurately described as mixed modes with a dominant spin direction. Consequently, the OH* response from underlying mixed mode contaminates the structure of the phase averaged OH*. However, we can extract the pure spinning response of the OH* fluctuations by employing a novel rotational averaging procedure.

This method takes advantage of previous observations that the global fluctuating OH* responds at the resonant frequency, does not exhibit harmonics, is approximately sinusoidal, and that in spinning modes the dynamic response of all flames is the same but with an offset in phase determined by the burner distance and resonant frequency [4]. The basic premise of the method is to conduct a spatial averaging in a frame of reference moving with the spinning wave in either direction.

We first assemble normalised phase averages: $\tilde{Q}_n = (\tilde{Q} - \overline{Q})/\langle\overline{Q}\rangle$, where $\tilde{Q} = \tilde{Q}(r, \theta, t)$ is the spatial distribution of OH* intensity captured by the camera, $\overline{Q} = \overline{Q}(r, \theta)$ is the time-averaged mean and $\langle\overline{Q}\rangle$ is the spatially ensembled time-average evaluated over the whole annulus. Therefore, $\tilde{Q}_n = \tilde{Q}_n(r, \theta, \tau/T)$, where τ/T is the normalised position in the phase averaged cycle.

For the general case of N burners, the normalised forcing cycle is divided into N time-steps for phase averaging ($N = 12$ herein). In order to isolate the spinning component in a given direction, the jth phase average field is rotated by an angle $\beta = 2\pi j/N$ against the given spin direction effectively *freezing* the spinning mode. The average of the N rotations distributions is then calculated according to Eq. 1, producing a single spatial spin compensated distribution, $\overline{Q}^{x}_{rot} = f(r, \theta)$. A schematic of the method is shown in Fig. 2.

$$\overline{Q}^{x}_{rot} = \frac{1}{N}\sum_{j=0}^{N-1} \mathrm{Rot}_{\beta_j}\left\{\left[\frac{\tilde{Q} - \overline{Q}}{\langle\overline{Q}\rangle}\right]_j\right\}, \qquad (1)$$

where x is either the ACW or the CW component, j is the phase average time step and Rot_{β_j} is a rotation of β_j around the center of the annulus. The angle is calculated as $\beta_j = \pm\frac{2\pi}{N}j$, where positive and negative signs are used for CW and ACW components respectively.

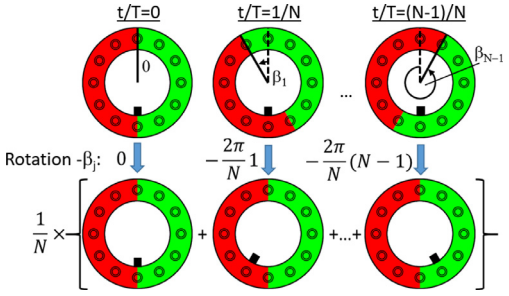

Fig. 2. Schematic of the rotational averaging method. The sector rotations, β_j, depicted in the figure are in the ACW direction as would be applied to an ACW spinning mode.

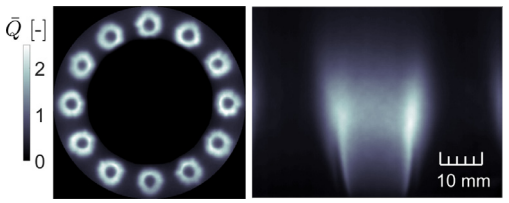

Fig. 3. Left: Overhead image of the mean OH*. Right: Side image of the mean OH*.

The method effectively decomposes OH* distribution into harmonic components by cancelling OH* fluctuations driven by pressure waves travelling in the opposite direction. An additional advantage is that small variations in the flames are also averaged out, providing a clearer description of the unsteady flame response to acoustic waves.

3. Results

3.1. Mean flame structure

Figure 3 shows the mean OH* chemiluminescence imaged from above and a picture from the side of one of the turbulent bluff-body flames. Compared with swirling flames reported in previous investigations [3–5], these flames are longer, more radially compact and remain isolated around the annulus as shown by the concentric OH* structure of all 12 flames. The flame is stabilised along the inner shear layer at the bluff body edge although a second lifted flame front is stabilised in the outer shear layer. It was previously observed that for the 12 burner swirling flame configuration the tops of the flame brushes were in close proximity to both neighbouring flames and the combustor walls [4].

3.2. Frequency and amplitude response

The frequencies of the self-excited azimuthal modes for different U_b and different values of ϕ are

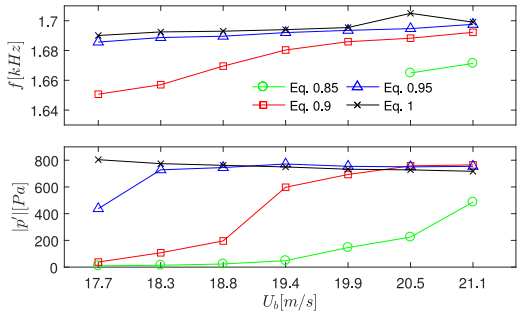

Fig. 4. Effect of ϕ and U_b on the self-excited instability frequency (top) and amplitude (bottom).

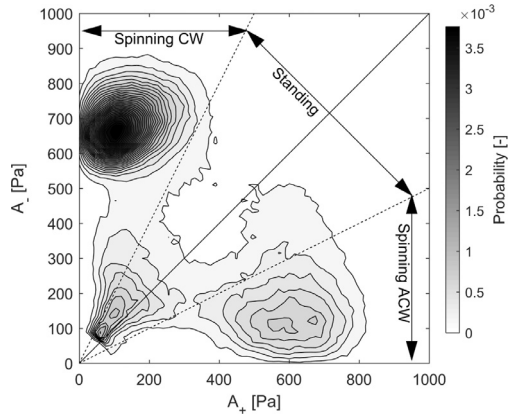

Fig. 5. Joint PDF of A_+ and A_- for all ϕ at $U_b =$ 19.9 m/s. Dashed lines from origin denote thresholded boundary of predominantly spinning and standing modes.

plotted in Fig. 4. The instability frequency of the first azimuthal mode lies between 1650 and 1710 Hz depending on the operating conditions. Overall the trends show that the instability frequency increases approximately linearly with increasing power and with increasing flame speed (increasing ϕ) as observed previously [3]. However, in the absence of swirl, the instability frequencies are approximately 50 Hz lower. The frequency difference equates to an approximate reduction in the mean gas temperature of $\Delta T \approx 115$K indicating that the temperature profile in the combustor is modified by the change in the flame shape compared with swirling flames.

Figure 4 (bottom) shows the stability map in terms of the mean pressure amplitude of the response in terms of ϕ and U_b. It shows that, in general, high amplitude instabilities are excited at richer equivalence ratios and higher thermal loads. It is interesting to note that there appears to be a well defined maximum pressure amplitude response, which may result from saturation of the instability at high amplitudes.

3.3. Mode characterisation

Figure 5 plots the joint probability density function (PDF) of A_+ and A_- for all ϕ at $U_b = 19.9$m/s. The joint PDF shows that the modal response is stochastic at low instability amplitudes, and bi-modal at higher amplitudes, with a statistical preference for CW spinning waves. This distribution is distinctly different to that observed in swirling flames, which did not exhibit a bi-modal response [3,4,8], but shows remarkably close agreement with theory of Schuermans et al. [12] who suggested a transition from standing to spinning waves when the amplitude of an instability increases. The high probability of exciting spinning modes in either direction can be attributed to the absence of swirl or mean azimuthal flow. We conjecture that the higher probability of exciting CW, as opposed to ACW, spinning modes is likely to arise from imperfections in geometric azimuthal symmetry or small flow non-uniformities as suggested by Sensiau [19].

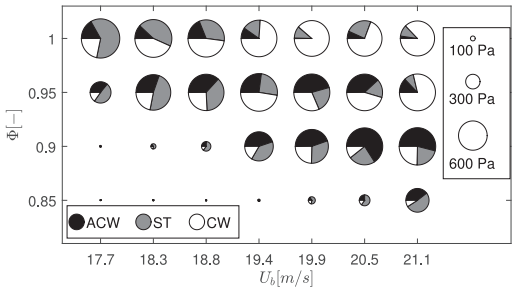

Fig. 6. Stability map showing modal content at each operating point. Note: circle diameter scales with the magnitude of the pressure fluctuations.

We note some general similarities to the results of Prieur et al. [17], who found that initial conditions determined the direction of self-excited spinning modes. The present findings appear to support this finding, albeit with the addition of bi-modal dynamics, which may be driven by the fully turbulent flow in the current configuration [1].

Figure 6 shows a stability map that also includes the modal content at each operating point. The diameter of the circles scale with the amplitude of the pressure fluctuations and are divided into pie graphs which show the proportion of predominantly spinning (in both directions) and standing modes according to the definition in Section 2.4. It is interesting to note that only the cases close to the onset boundary of high amplitude instabilities appear to show stochastic behaviour and a predominantly standing behaviour, but at higher ϕ and U_b conditions spinning modes are observed more frequently. The small fractions of predominantly standing waves that are observed during bi-modal behaviour occur mainly during the switching transition between CW and ACW states.

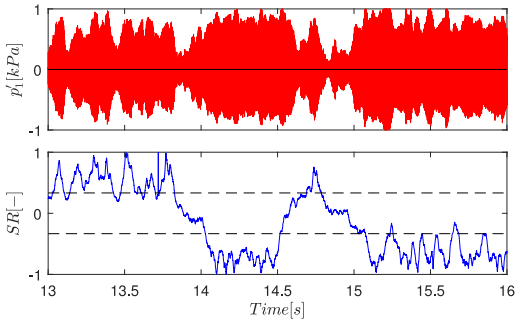

Fig. 7. Top: Pressure time-series showing modal dynamics. Bottom: Time-series of the spin ratio SR evaluated from the pressure data. Dashed lines correspond to thresholds use to classify modes: $SR > 1/3$ are classified as ACW spinning modes, $SR < -1/3$ are classified as CW spinning modes intermediate values are classed as standing modes.

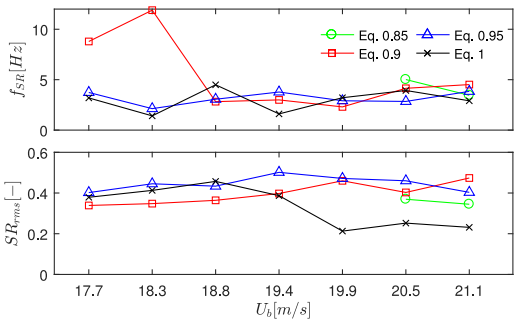

Fig. 8. Top: Frequency of the spin ratio time-series for different values of U_b and ϕ. Bottom: *r.m.s* fluctuations of the SR time-series for different values of U_b and ϕ.

3.4. Modal dynamics

We now consider the time-varying nature of the self-excited modes in more detail. Figure 7 (top) shows a typical pressure time-series recorded at location *p1* for the case where $\phi = 0.95$ and $U = 19.9$ m/s. Figure 7 (bottom) shows the time-series of the SR evaluated from the pressure time-series. The pressure time series shows low frequency modulations, relative to the instability frequency, of the amplitude envelope which is characteristic feature of mode switching. The mode switching is quantified by the SR time-series which shows that the mode of oscillation is constantly oscillating experiencing low amplitude oscillations in spin ratio. The mode can also be observed to periodically switch from strongly spinning in the ACW to the CW direction and vice versa, passing through predominantly standing modes during each switch. Excursions of the SR above the top dashed line and below the bottom dashed line are classified as spinning modes whereas points in-between are classified as predominantly standing. The observed low frequency switching of the SR and the low frequency modulations of the pressure time series are qualitatively similar, however their time-scales are orders of magnitude longer than the instability.

Figure 8 plots the low frequency modulation of the SR (top) and the *r.m.s* of the SR modulations (bottom), evaluated using a similar approach to [8]. The frequency range of the mode switching in terms of SR is between $2 - 11$ Hz, but overall mode switching occurs at a relatively constant frequency of around 4 Hz and appears to be independent of both ϕ and U_b. The slow time-scale of the mode-switching is of the order of the convective velocities but the mechanism that drives this low frequency behaviour is at present not understood. It should also be noted that this behaviour is notably different from swirling flames where the oscillation frequency was observed to increase with ϕ [8].

Figure 8 (bottom) shows that the magnitude of the spin ratio fluctuations remains relatively constant at $SR_{rms} \approx 0.3 - 0.5$ for the majority of cases. It is only the $\phi = 1$ cases which show a reduction in the rms value with increasing U_b. This occurs when the periodic switching from CW to ACW modes occurs less often, and the mode appears to settle in a preferred state.

3.5. Fluctuating heat release rate

In this section we consider the periodic structure of the fluctuating heat release rate obtained from high speed OH* imaging using phase averages as well as a new rotational averaging procedure described earlier in Section 2.4. We are particularly interested in understanding how the spatial structure and dynamics of the global fluctuating heat release rate of isolated turbulent flames respond to spinning waves and whether the response is the same in both spin directions. We conjecture that in the absence of swirl and bulk azimuthal flow the structure of the OH* fluctuations should be similar.

Figure 9 shows 6 non-dimensional time-steps, t/T, of the standard phase averaged images of the fluctuating component of the heat release rate for an ACW mode where $\phi = 0.95$ and $U = 19.9$ m/s. At $t/T = 0$ we see peak values of the OH* fluctuations, shown in red, in the bottom right hand quadrant and negative OH* fluctuations (mean is set to zero), shown in blue, diametrically opposite. This structure rotates around the annulus over the duration of the cycle. The turbulent bluff body flames have a low cone angle which means that a stable flame appears as a concentric region of peak OH* chemiluminescence as shown in Fig. 3. The phase averaged images of the ACW spinning mode in Fig. 9 show that the regions of maximum and minimum OH* form crescent shaped structures on opposite sides of the flame. As an observer sitting on the bluff body and looking inwards, the larger

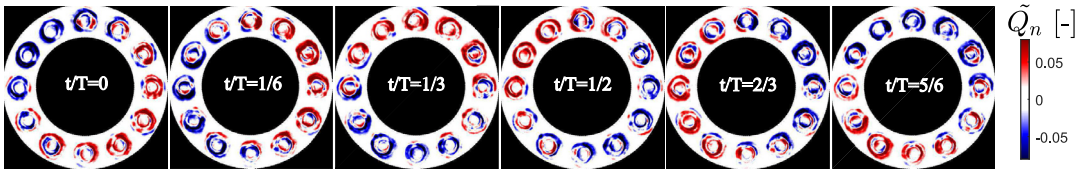

Fig. 9. Phase averaged overhead OH* chemiluminescence conditioned for spinning ACW at $\phi = 0.95$ and $U = 19.9$ m/s.

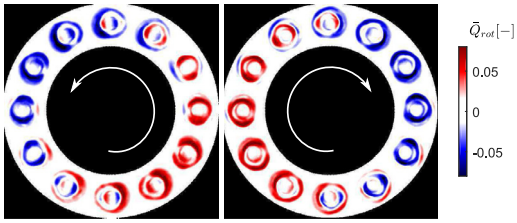

Fig. 10. Rotating average of the phase averaged overhead OH* chemiluminescence conditioned for spinning $\overline{Q}_{\mathrm{rot}}^{\mathrm{ACW}}$ (left) and $\overline{Q}_{\mathrm{rot}}^{\mathrm{CW}}$ (right). $\phi = 0.95$, $U = 19.9$ m/s.

crescent shaped regions of maximum OH* appear on the right hand side of the flame relative to the spinning wave, whereas the minimum OH* crescents appear on the left hand side. These features are particularly clear in $t/T = 1/6$ and 1/3.

Since near perfect spinning modes rarely occur, as shown in the joint PDF in Fig. 6 and the SR time-series in Fig. 8, the OH* responses from mixed mode components are present in the structure of the phase averaged OH*. However, we can extract the harmonic component of the OH* fluctuations produced by the spinning wave by employing the novel rotational averaging procedure described earlier.

The result of the rotational averaging procedure carried out for both CW and ACW spinning modes is shown in Fig. 10 as $\overline{Q}_{\mathrm{rot}}^{\mathrm{ACW}}$ (left) and $\overline{Q}_{\mathrm{rot}}^{\mathrm{CW}}$ (right). Despite minor differences in response amplitude, spin ratio and convergence the same features can be readily observed during both ACW and CW modes. Looking at the ACW mode, we see that the maximum and minimum OH* fluctuations show asymmetric ring like structures which spread radially outwards from the centre of each burner. The formation of these structures can be attributed to both the axial oscillation of the flow rate into the combustor and the transverse velocity oscillation resulting from the spinning pressure wave. Although the formation mechanism is generally similar to that of swirling flames (for example see ref. [5]), the response of the flames in the current configuration has a number of important differences.

Firstly, the absence of swirl reduces the spreading rate resulting in flames which are fully isolated from each other. Secondly, the fluctuating OH* structures, which are correlated to the roll-up of vortex structures on the shear layers, do not rotate locally around each bluff body as they advect downstream as found in swirling flames [3,5]. Both of these features make it more straightforward to unambiguously investigate the heat release rate response. The ring like fluctuating OH* structures are clearly asymmetric in terms of width and oscillation magnitude, with larger oscillations present on the sides of the flame aligned in the azimuthal direction. Moreover, the largest magnitude oscillation is observed on the side of the flame facing away from the incoming pressure wave. This is the opposite side of the flame in comparison with the response of swirling flames in [5], and may result from either vorticity cancellation [15], shear sheltering, or the absence of axially propagating vorticity waves [16] which may change the timing of the flame sheet dynamics although without access to the velocity field this remains a conjecture. While the source of the oscillation asymmetry remains uncertain, the fact that the largest asymmetries are aligned with the azimuthal direction suggest that the radial asymmetry observed in swirling flames [5] may be simply a result of these structures rotating locally around each bluff body as they advect downstream. This provides a possible explanation for the different spatial distribution of the fluctuating OH* structures around the annulus observed in previous studies [3].

It is also worth noting that at a number of points in the cycle (for example the flame at 7 o' clock on the CW mode image), multiple oscillations appear to be present simultaneously, with inner and outer ring or crescent like structures. For the inner set of structures, the orientation of the maximum and minimum values of the crescent shaped regions are on occasion reversed in comparison with the outer set. This structure is consistent with occurrence of transverse fluctuations giving rise to *flapping* motions of the flame brush, producing a staggered arrangement of azimuthally plane-symmetric structures rather than axisymmetric structures.

4. Conclusion

In this paper we have demonstrated experimentally that self-excited azimuthal modes can be excited in an annular combustor using turbulent bluff body flames without swirl, enabling us to better understand the time-varying nature of azimuthal

modes and the structure of the fluctuating heat release rate. Simultaneous pressure measurements and high speed OH* chemiluminescence were obtained for a range of operating conditions and showed that self-excited instabilities occur over a wide range of conditions. Stability maps and joint probability density functions of the instability amplitudes show that azimuthal modes are stochastic at low equivalence ratios showing similar probabilities for spinning, standing and mixed modes, but exhibit bimodal behaviour at higher equivalence ratios and velocities, preferring instead spinning modes. These features are significantly different to the behaviour of self-excited azimuthal modes with turbulent swirling flames. A new rotational averaging method to extract the harmonic components of the fluctuating heat release rate was presented and used to process high speed OH* images and analyse the structure of the OH* fluctuations for spinning modes. It was found that the structure of the fluctuating heat release rate of spinning modes is highly asymmetric and characterised by crescent shaped regions of peak OH* that are preferentially oriented according to the direction of spin and are observed on approximately half of the flames around the annulus. The same structure is observed in both spin directions but with opposite handedness.

Acknowledgements

This work was funded by the European Research Council (ERC) under the European Union's Horizon 2020 research and innovation programme (grant agreement no 677931 TAIAC). We also thank the technical staff of NTNU EPT for their support.

References

[1] N. Noiray, B. Schuermans, *Proc. R. Soc. A Math. Phys. Eng. Sci.* 469 (2012).
[2] J.F. Bourgouin, D. Durox, J.P. Moeck, T. Schuller, S. Candel, *Self-Sustained Instabilities in an Annular Combustor Coupled by Azimuthal and Longitudinal Acoustic Modes* (2013), doi:10.1115/GT2013-95010.
[3] N.A. Worth, J.R. Dawson, *Proc. Combust. Inst.* 34 (2013) 3127–3134.
[4] N.A. Worth, J.R. Dawson, *Combust. Flame* 160 (2012) 2476–2489.
[5] J.R. Dawson, N.A. Worth, *Combust. Flame* 161 (2014) 2565–2578.
[6] W. Krebs, P. Flohr, B. Prade, S. Hoffmann, *Comb. Sc. Tech.* 174 (2002) 99–128.
[7] G. Ghirardo, M.P. Juniper, *Proc. R. Soc. A Math. Phys. Eng. Sci.* 469 (2013).
[8] N.A. Worth, J.R. Dawson, *Proc. Combust. Inst.* 36 (2017) 3743–3751.
[9] N.A. Worth, J.R. Dawson, J.A.M. Sidey, E.M. Mastorakos, *Proc. Combust. Inst.* 36 (2017) 3783–3790.
[10] P. Wolf, G. Staffelbach, L.Y.M. Gicquel, J.D. Müller, T. Poinsot, *Combust. Flame* 159 (2012) 3398–3413.
[11] B. Schuermans, V. Bellucci, C.O. Paschereit, *Non-Linear Combustion Instabilities in Annular Gas-Turbine Combustors*, American Institute of Aeronautics and Astronautics, 2006, doi:10.1115/GT2013-95010.
[12] B. Schuermans, V. Bellucci, C.O. Paschereit, *Thermoacoustic Modeling and Control of Multi Burner Combustion Systems* (2003), doi:10.1115/GT2003-38688.
[13] M.R. Bothien, N. Noiray, B. Schuermans, *J. Eng. Gas Turbines Power* 137 (2015) 061505.
[14] J.F. Bourgouin, D. Durox, J.P. Moeck, T. Schuller, S. Candel, *J. Eng. Gas Turbines Power* 137 (2015) 021503.
[15] R. Sau, K. Mahesh, *JFM* 604 (2008) 389–409.
[16] P. Palies, D. Durox, T. Schuller, S. Candel, *Combust. Flame* 157:9 (2010) 1698–1717.
[17] K. Prieur, D. Durox, T. Schuller, S. Candel, *Combust. Flame* 175 (2017) 283–291.
[18] M. Bauerheim, M. Cazalens, T. Poinsot, *Proc. Combust. Inst.* 35 (2015) 3219–3227.
[19] C. Sensiau, F. Nicoud, T. Poinsot, *Int. J. Aeroacoust.* 8 (1) (2009) 57–67.